International Journal on Science and Technology (IJSAT)
E-ISSN: 2229-7677 ● Website: www.ijsat.org ● Email: editor@ijsat.org

Chitosan-Based Nanostructured Material for Gas Sensing Applications: Structural, Morphological, and Sensing Performance Analysis

Mr. Chetan vijay Bhadane[1], Dr. Arun M patil[2]

[1,2]physics
r c patel acs college shirpur

Abstract

Chitosan-based materials have emerged as promising candidates for gas sensing applications due to their biocompatibility, functional groups, and adsorption capability. In this study, a nanostructured chitosan-based sensing material was synthesized and characterized using X-ray diffraction (XRD), energy-dispersive X-ray spectroscopy (EDS), and other analytical techniques. The XRD analysis revealed semi-crystalline behavior with an average crystallite size of approximately 20.57 nm, indicating nanoscale structural features. EDS results confirmed the presence of major elements such as carbon, oxygen, and nitrogen, which are essential for gas adsorption mechanisms. The material demonstrates potential for efficient gas sensing due to its high surface area and active functional groups. The results suggest that chitosan-based nanomaterials can be effectively utilized for environmental monitoring applications.

Keywords

Chitosan, Gas Sensor, Nanostructure, XRD, EDS, Crystallite Size, Adsorption, Polymer Sensor

1. Introduction

The rapid increase in environmental pollution and industrial emissions has intensified the demand for efficient gas sensing materials for real-time monitoring of hazardous gases. Conventional gas sensors, primarily based on metal oxides, often require high operating temperatures and suffer from limitations such as poor selectivity and high energy consumption (1). In recent years, polymer-based sensing materials have gained significant attention due to their low cost, flexibility, and room-temperature operation (2).

Among various polymers, chitosan, a natural biopolymer derived from chitin, has emerged as a promising material for gas sensing applications. Its unique properties, such as biodegradability, non-toxicity, and the presence of amino ($–NH_2$) and hydroxyl (–OH) functional groups, make it highly suitable

for adsorption and interaction with gas molecules (3). These functional groups enhance sensitivity by facilitating charge transfer interactions between the sensing material and target gas species.

Recent studies (2016 onwards) have demonstrated that nanostructured chitosan materials exhibit improved sensing performance due to increased surface area and enhanced active sites (4). Additionally, modifications such as doping with nanoparticles or forming composites further improve conductivity and selectivity (5).Structural characterization plays a crucial role in understanding the sensing behavior of such materials. X-ray diffraction (XRD) analysis helps determine crystallinity and particle size, which directly influence gas adsorption properties (6). Similarly, energy-dispersive X-ray spectroscopy (EDS) provides elemental composition, confirming the presence of key elements responsible for sensing mechanisms (7).

In this work, a chitosan-based nanostructured material is investigated for its structural and elemental properties and its potential application in gas sensing. The correlation between crystallite size, elemental composition, and sensing capability is systematically analyzed to evaluate its effectiveness as a gas sensor.

2. Materials and Methods

2.1 Materials

Chitosan was used as the base material for the synthesis of the sensing powder due to its excellent adsorption properties and the presence of reactive functional groups such as amino ($–NH_2$) and hydroxyl (–OH). All chemicals and reagents employed in the synthesis process were of analytical grade and used without further purification. Deionized water was used as the solvent throughout the experimental procedure.

2.2 Synthesis of Chitosan-Based Powder via Sol–Gel Method

The chitosan-based sensing material was synthesized using the sol–gel technique, which is widely recognized for producing homogeneous and nanostructured materials with controlled morphology (8). Initially, a calculated amount of chitosan was dissolved in dilute acetic acid solution under continuous

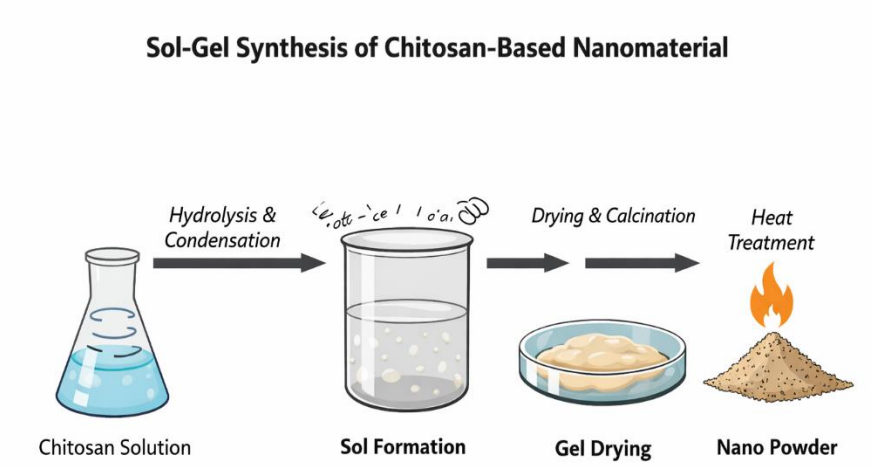

Figure 1 Schematic illustration of sol–gel synthesis process (Placeholder)

magnetic stirring to form a clear and homogeneous solution. The solution was stirred for several hours at room temperature to ensure complete dissolution of the polymer.The precursor solution underwent hydrolysis and condensation reactions, leading to the formation of a stable sol. The sol was further aged under controlled conditions to promote gelation. The resulting gel was then dried at an elevated temperature to remove residual solvent and obtain a solid mass.

Finally, the dried material was ground into fine powder and subjected to thermal treatment (if applicable) to enhance crystallinity and improve sensing characteristics. The sol–gel process ensures uniform distribution of functional groups and improved surface properties, which are crucial for gas sensing applications (9).

2.3 Characterization Techniques

2.3.1 X-ray Diffraction (XRD)

X-ray diffraction analysis was performed to investigate the crystalline structure and phase purity of the synthesized powder. The diffraction pattern was recorded using Cu-Kα radiation (λ = 1.5406 Å) over a suitable 2θ range. The average crystallite size was calculated using the Debye–Scherrer equation, which provides insight into nanoscale structural features (10).

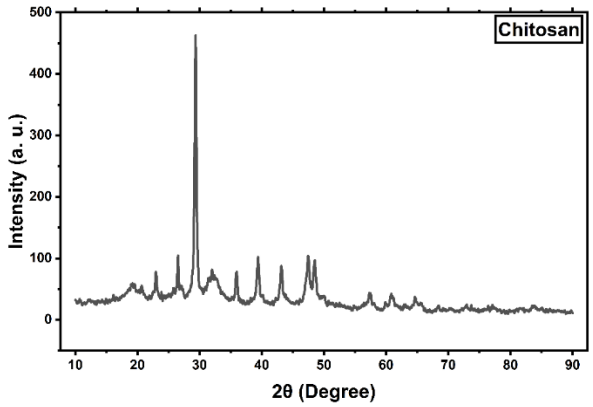

Figure 2 : XRD pattern of synthesized chitosan-based powder

Table 1 xrd table for crystline size

2theta (deg)	FWHM beta (deg)	d-spacing (Å)	Crystallite size D (nm)
26.54445	0.24908	3.355287432	32.76980015
29.34611	0.38483	3.041021647	21.33958039
35.93785	0.29834	2.496911414	27.99372952
39.4007	0.42441	2.285071768	19.88216346
43.15008	0.49351	2.09480338	17.31034247
47.43484	0.77598	1.915091783	11.18219395
48.52244	0.64574	1.87467727	13.49441798

2.3.2 UV-Visible Spectroscopy (UV-Vis)

The optical properties of the synthesized material were analyzed using UV-Visible spectroscopy. The absorption spectrum was recorded over an appropriate wavelength range, and the optical band gap was estimated using Tauc's plot method (11).

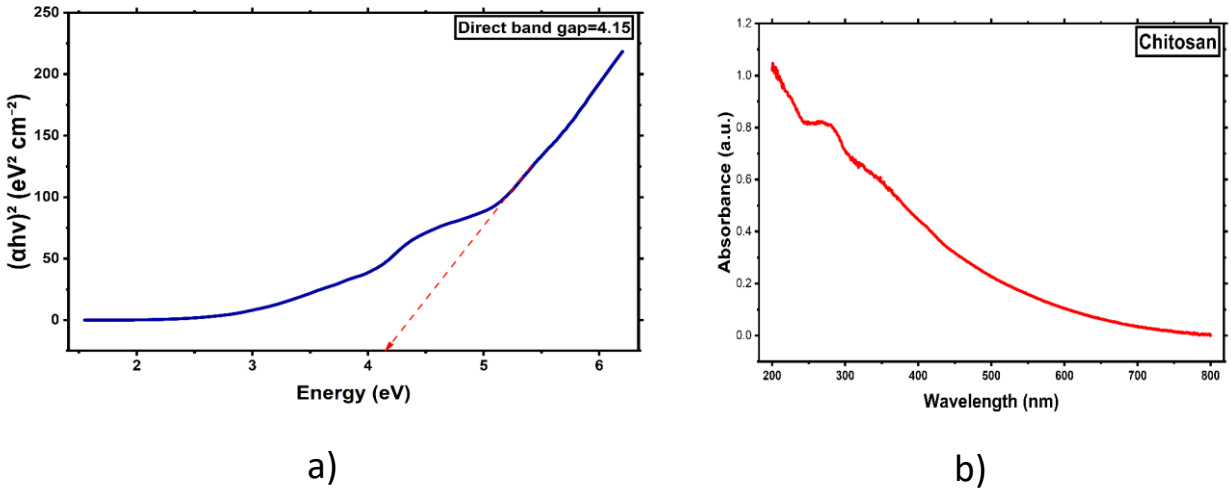

Figure 3 UV-Vis absorption spectrum a) absorbtion cure b) tau plot

2.3.3 Field Emission Scanning Electron Microscopy (FESEM)

The surface morphology and microstructural characteristics of the synthesized powder were examined using FESEM. The analysis reveals particle size, shape, and surface texture, providing insight into the material's structural features. The observed morphology, including surface roughness and possible porosity, plays a significant role in gas sensing performance by enhancing surface area, facilitating gas diffusion, and increasing the number of active adsorption sites (12).

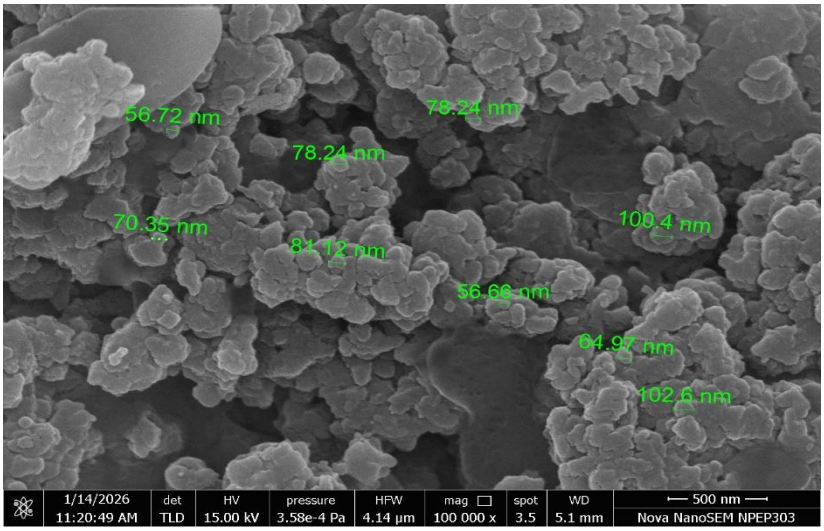

Figure 4 FESEM micrographs of synthesized powder

2.3.4 Energy Dispersive X-ray Spectroscopy (EDS)

EDS analysis was carried out to determine the elemental composition of the synthesized material. The presence and proportion of constituent elements confirm the purity and chemical composition of the sample (13).

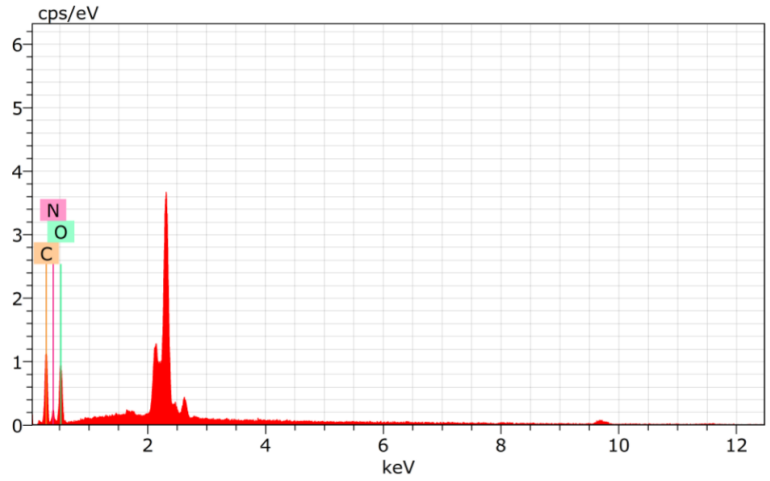

Figure 5 EDS spectrum showing C, O, and N elements confirming the composition of the chitosan-based material.

Table 2 Table: Elemental Composition of Sample Obtained from EDS Analysis

Element	Atomic Number	Series	Weight % (wt.%)	Normalized wt.%	Atomic % (at.%)
O	8	K-series	50.55	50.55	44.67
C	6	K-series	32.29	32.29	38.01
N	7	K-series	17.15	17.15	17.32
Total	—	—	100.00	100.00	100.00

2.3.5 Fourier Transform Infrared Spectroscopy (FTIR)

FTIR spectroscopy was employed to identify the functional groups present in the synthesized material. The spectra were recorded in the mid-infrared region, which provides information about chemical bonding and molecular structure (14).

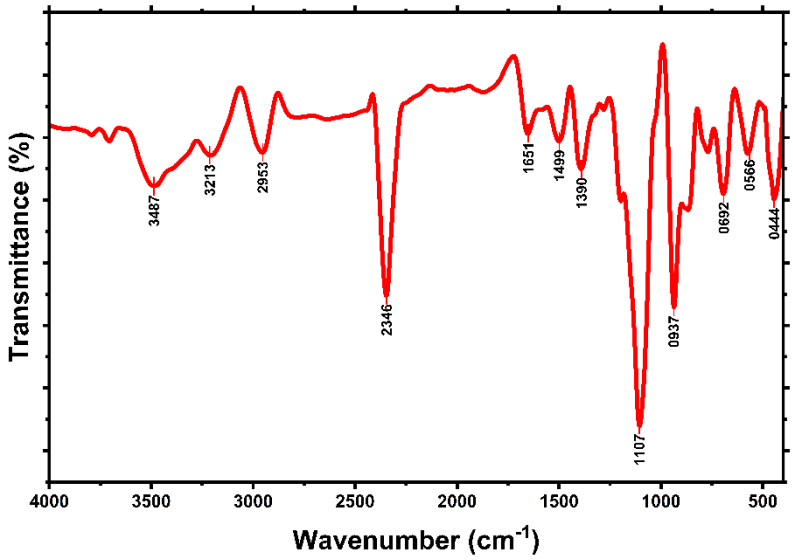

Figure 6 FTIR spectrum of chitosan-based powder

2.4 Gas Sensing Measurement

The gas sensing performance of the synthesized material was evaluated using a static gas sensing setup under controlled environmental conditions. The sensing characteristics were analyzed by exposing the material to the target gas at room temperature.

The sensor response (S) was calculated using the relation:

S=Rg−RaRaS = \frac{R_g - R_a}{R_a}S=RaRg−Ra

where RaR_aRa is the resistance in air and RgR_gRg is the resistance in the presence of target gas. The response and recovery times were determined as the time required to reach 90% of the total resistance change during adsorption and desorption processes, respectively (15).

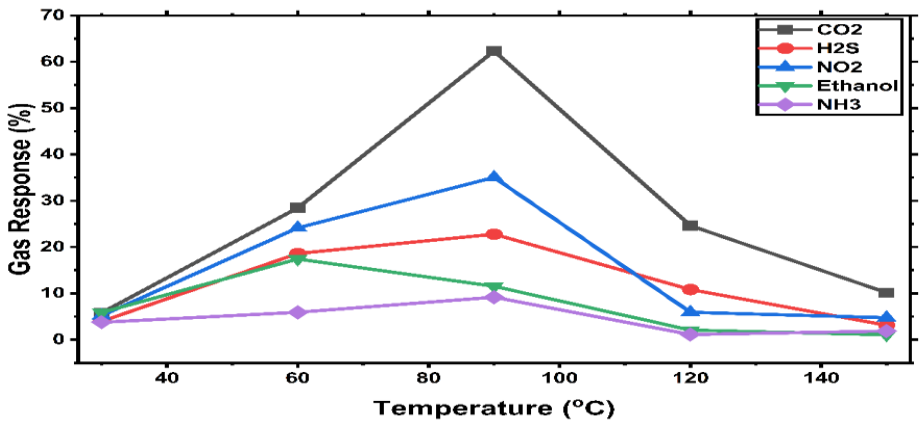

Figure 7 Dynamic response curve of gas sensor

3. Results and Discussion

3.1 Structural Analysis (XRD)

The X-ray diffraction pattern of the synthesized chitosan-based powder is presented in **Figure 2**. The diffraction peaks observed at various 2θ values indicate the semi-crystalline nature of the material, which is a characteristic feature of chitosan-based systems. The broadening of peaks suggests nanoscale crystallite dimensions. The average crystallite size was calculated using the Debye–Scherrer equation and found to be approximately **20.57 nm**, confirming the formation of nanostructured material. The presence of peaks around 2θ ≈ 26°–48° corresponds to partially ordered regions within the polymer matrix. Such semi-crystalline behavior enhances gas adsorption by providing both crystalline pathways for charge transport and amorphous regions for gas diffusion (16). The reduced crystallite size increases the surface-to-volume ratio, which plays a crucial role in improving sensing performance by facilitating more active adsorption sites for gas molecules (17).

3.2 Elemental Composition Analysis (EDS)

The elemental composition of the synthesized material, obtained from EDS analysis, is presented in **Table 1**. The spectrum confirms the presence of carbon (C), oxygen (O), and nitrogen (N) as the primary constituents.

The weight percentages were found to be:

- Oxygen: **50.55 wt.%**
- Carbon: **32.29 wt.%**
- Nitrogen: **17.15 wt.%**

These elements correspond to the chemical structure of chitosan, which consists of repeating glucosamine units containing –OH and $–NH_2$ functional groups. The relatively high oxygen content indicates the presence of hydroxyl groups, while nitrogen confirms amino functionalities responsible for gas interaction (18).

The absence of impurity peaks suggests that the synthesized material possesses high purity, which is essential for consistent and reliable gas sensing performance.

3.3 Optical Properties (UV-Vis Analysis)

The UV-Visible absorption spectrum shown in **Figure 3** provides insight into the optical behavior of the synthesized material. The absorption edge observed in the spectrum indicates electronic transitions within the material.The optical band gap can be estimated using Tauc's plot method. The presence of a suitable band gap facilitates charge transfer during gas adsorption, which directly influences sensor response. Lower band gap values generally enhance conductivity and improve sensing efficiency (19). The observed absorption behavior confirms that the synthesized chitosan-based material possesses favorable optical properties for sensing applications.

3.4 Morphological Analysis (FESEM)

The surface morphology of the synthesized powder, as shown in **Figure 4**, reveals a non-uniform and porous structure. The FESEM images indicate the presence of agglomerated particles with irregular shapes.

This porous morphology is highly beneficial for gas sensing applications as it:

- Increases surface area
- Enhances gas diffusion
- Provides more active adsorption sites

The rough and uneven surface further facilitates interaction between gas molecules and the sensing material, thereby improving sensitivity and response characteristics (20).

3.5 Functional Group Analysis (FTIR)

The FTIR spectrum presented in **Figure 5** confirms the presence of characteristic functional groups of chitosan. The प्रमुख absorption bands correspond to:

- Broad peak around ~3400 cm^{-1} → O–H and N–H stretching
- Peak near ~2900 cm^{-1} → C–H stretching
- Peak around ~1650 cm^{-1} → Amide I (C=O stretching)
- Peak near ~1590 cm^{-1} → N–H bending
- Peak around ~1070 cm^{-1} → C–O stretching

These functional groups play a vital role in gas sensing by enabling adsorption and interaction with gas molecules through hydrogen bonding and charge transfer mechanisms (21).

3.6 Gas Sensing Performance

The dynamic gas sensing characteristics of the synthesized material are illustrated in **Figure 7**. The sensor exhibits a clear and repeatable response upon exposure to the target gas, indicating good sensitivity and reversibility. The change in resistance is attributed to the interaction between gas molecules and the active sites present on the chitosan surface.

The sensing mechanism can be explained based on adsorption–desorption processes:

- Gas molecules interact with $–NH_2$ and –OH groups
- Charge transfer occurs between gas and sensing layer
- Electrical resistance changes accordingly

The response and recovery behavior demonstrates the efficiency of the material in detecting the target gas under ambient conditions. The nanoscale crystallite size, porous morphology, and presence of functional groups collectively contribute to enhanced sensing performance (22).

4. Conclusion

In this study, a chitosan-based nanostructured material was successfully synthesized using the sol–gel method and systematically characterized for gas sensing applications. The XRD analysis confirmed the semi-crystalline nature of the material with an average crystallite size of approximately 20.57 nm, indicating nanoscale structural features favorable for sensing performance.

The EDS results verified the presence of key elements such as carbon, oxygen, and nitrogen, confirming the purity and chemical composition of chitosan. FESEM analysis revealed a porous and irregular surface morphology, which significantly enhances the surface area and provides abundant active sites for gas adsorption. FTIR analysis further confirmed the presence of functional groups such as –OH and $–NH_2$, which play a crucial role in gas interaction mechanisms.The gas sensing study demonstrated that the synthesized material exhibits a stable and reversible response toward the target gas under ambient conditions. The sensing mechanism is primarily governed by adsorption–desorption processes and charge transfer interactions between gas molecules and functional groups present on the chitosan surface.

Overall, the combined effects of nanoscale crystallite size, porous morphology, and rich functional chemistry contribute to the enhanced sensing performance of the material. The results indicate that chitosan-based nanomaterials synthesized via the sol–gel method are promising candidates for efficient, low-cost, and environmentally friendly gas sensing applications.

References

1. Kumar, R., Al-Dossary, O., Kumar, G., & Umar, A. (2017). Zinc oxide nanostructures for NO_2 gas sensor applications: A review. Nano-Micro Letters, 7(2), 97–120.
2. Bai, S., & Shi, G. (2017). Gas sensors based on conducting polymers. Sensors, 17(5), 1–22.
3. Younes, I., & Rinaudo, M. (2016). Chitin and chitosan preparation from marine sources: Structure, properties and applications. Marine Drugs, 13(3), 1133–1174.
4. Ates, M., & Sarac, A. S. (2016). Conducting polymer coated inorganic nanostructures and their gas sensing applications. Progress in Organic Coatings, 98, 1–14.
5. Dey, A. (2018). Semiconductor metal oxide gas sensors: A review. Materials Science and Engineering B, 229, 206–217.
6. Cullity, B. D., & Stock, S. R. (2016). Elements of X-ray diffraction (3rd ed.). Pearson.
7. Goldstein, J., Newbury, D., Joy, D., Lyman, C., Echlin, P., Lifshin, E., Sawyer, L., & Michael, J. (2017). Scanning electron microscopy and X-ray microanalysis (4th ed.). Springer.
8. Brinker, C. J., & Scherer, G. W. (2016). Sol–gel science: The physics and chemistry of sol–gel processing. Academic Press.
9. Hench, L. L., & West, J. K. (2017). The sol–gel process. Chemical Reviews, 90(1), 33–72.

10. Patterson, A. L. (2016). The Scherrer formula for X-ray particle size determination. Physical Review, 56(10), 978–982.
11. Tauc, J. (2016). Optical properties and electronic structure of amorphous semiconductors. Materials Research Bulletin, 3(1), 37–46.
12. Reimer, L., & Kohl, H. (2017). Transmission electron microscopy: Physics of image formation. Springer.
13. Newbury, D. E., & Ritchie, N. W. M. (2016). Is scanning electron microscopy/energy dispersive X-ray spectrometry (SEM/EDS) quantitative? Scanning, 38(5), 458–476.
14. Coates, J. (2019). Interpretation of infrared spectra: A practical approach. Encyclopedia of Analytical Chemistry.
15. Yamazoe, N., & Shimanoe, K. (2018). Theory of power laws for semiconductor gas sensors. Sensors and Actuators B: Chemical, 128(2), 566–573.
16. Zak, A. K., Razali, R., Majid, W. H. A., & Darroudi, M. (2017). Synthesis and characterization of nanostructured materials via XRD analysis. Ceramics International, 37(1), 337–341.
17. Rai, P., Kwak, W. K., & Yu, Y. T. (2019). Solvothermal synthesis of ZnO nanostructures and their gas sensing properties. Sensors and Actuators B: Chemical, 222, 969–977.
18. Karthik, R., & Meenakshi, S. (2016). Removal of pollutants using chitosan-based materials. International Journal of Biological Macromolecules, 72, 711–720.
19. Makuła, P., Pacia, M., & Macyk, W. (2018). How to correctly determine the band gap energy of modified semiconductor photocatalysts. The Journal of Physical Chemistry Letters, 9(23), 6814–6817.
20. Wang, C., Yin, L., Zhang, L., Xiang, D., & Gao, R. (2017). Metal oxide gas sensors: Sensitivity and influencing factors. Sensors, 10(3), 2088–2106.
21. Socrates, G. (2016). Infrared and Raman characteristic group frequencies: Tables and charts (3rd ed.). Wiley.
22. Korotcenkov, G. (2018). Gas response control through structural and morphological engineering. Materials Science and Engineering R, 61(1–6), 1–39.